Desalination and Water Treatment
www.deswater.com
doi: 10.1080/19443994.2015.1058725

57 (2016) 12977–12987
June

Taylor & Francis
Taylor & Francis Group

CFD modeling and analysis of brine spray evaporation system

Lei Chen[a,b], Xuening Fei[a,b,*], Yuman Dai[c], Min Ji[b], Hongwei Zhang[b], Xiumei Jiao[a]

[a]*School of Environmental and Municipal Engineering, Tianjin Chengjian University, Tianjin, China, Tel. +86 02223773363; email: lucu2005@gmail.com (L. Chen), Tel. +86 02223773360; emails: xueningfei@126.com (X. Fei), lmjxm@163.com (X. Jiao)*
[b]*School of Environmental Science and Engineering, Tianjin University, Tianjin, China, Tel. +8602223773360; emails: jimin@tju.edu.cn (M. Ji), hwzhang@tju.edu.cn (H. Zhang)*
[c]*School of Energy and Safety Engineering, Tianjin Chengjian University, Tianjin, China, Tel. +8602223773363; email: daiyuman88@126.com*

Received 21 August 2014; Accepted 26 May 2015

ABSTRACT

A spraying evaporation system applied to brine disposal is reported, which is mainly used for disposing the brine with concentration more than 100,000 mg/L. A computational fluid dynamics (CFD) simulation has been carried out to study the brine droplet evaporation and diffusion process in high temperature air flow. A discrete-phase model in spraying evaporation system is developed and a simulation experiment based on the gas–liquid phrase coupling with hydromechanics theory is conducted, respectively. In the present study, this model is further verified by comparing simulated temperature with experimental temperature under the condition of feed rate at 11, 13, and 15 L/h, respectively, hot air flux at 78 m^3/h, temperature at 260°C, and compressed air pressure at 0.2 MPa. It should be pointed out that the CFD results are in reasonable agreement with experimentally measured ones. A thorough analysis of the heat- and mass-transfer in controlling steps is conducted based on this model to determine the impacts of key parameters that could contribute to an enhanced spray evaporation system, and finally find out the optimized operating condition. Several operating parameters, including air pressure given by air compressor, temperature and flux of hot air, and feed rate of brine are investigated to examine their effects on the evaporation (E) and the evaporation rate (R). The results show that the optimized operating condition of spraying system is air pressure at 0.3 MPa, hot air temperature at 270°C, hot air flux at 64 m^3/h, and brine feed rate at 11 L/h.

Keywords: Desalination; Spray evaporation; Computational fluid dynamics; Process enhanced; Brine

1. Introduction

Brine generated in desalination refers to high concentration solution with salinity (measured by sodium chloride) more than 3.5% (W/W) [1], which is always the residual of original solution after some fresh water evaporated. With the rapid development of economy, more and more industries produce brine [2], such as seawater desalination, municipal sewage treatment plant, various industrial desalination including electric power, oil–gas, mining and metallurgical as well as chemical industries. Although, a large investment in

*Corresponding author.

desalination eases the water crisis and promotes the global economy in a certain degree, simultaneously it produces large quantity of brine by-product. Traditional approaches to brine disposal include direct discharge [3], using evaporation ponds and deep wells, etc.

In recent years, the impacts of brine effluent discharge on ecological environment have been investigated. It is believed that the residual chemical toxicity of discharging brine can cause potential threats to ecological environment [4,5]. Therefore, many brine effluent desalination processes have been developed to achieve the goal of resource recycling [3] and zero pollution discharge [6]. So far, the brine effluent produced by seawater desalination can be treated with some process, such as thermal, membrane separation process, electrodialysis (ED), ion exchange, eutectic freezing crystallization, and chemical processes, etc. However, they are all companied with high operating cost, high-energy consumption, and are easy to scale. Therefore, it is necessary to find out a novel process with high brine recovery and concentration rate.

Some researchers [7–9] suggested spray evaporation technology to be applied to brine disposal because of its advantages of high concentration rate, no fouling, and especially for high concentration brine. The mechanism is that the brine was sprayed and evaporated immediately in the surrounding of hot air, followed by water vapor separating from brine, and condensed for recovery afterwards. The concentration of the resulted residual could be 20 times higher than that of the initial. By this means, we can both solve the problem of brine disposal and lower the production cost.

Water spray encounters with hot air in the vertical district of spray tower, where it exists in both mass-transfer and complicated momentum and energy-transfer. Thus, the stream of brine droplet and hot air is a complex multiphase turbulent flow, which can be affected by many parameters in phase change process. It is well recognized that four factors, including the hot air and the feed flux, hot air temperature, and air pressure, play important roles in spray evaporation performance [10]. Therefore, it is essential to model the temperature field during brine spray evaporation process and develop methods to predict experimental results and optimize the operating conditions.

Computational fluid dynamics (CFD) has been widely applied in desalination field and proved to be a valuable tool in analyzing fluid dynamic behavior. With the benefits of visualizing the flow field at any location in a defined flow channel, CFD modeling can be used to analyze key process design, determine the controlling step in mass- and heat-transfer process and provide guidance for scaleup. Many researchers have used CFD to analyze the desalination process, such as direct contact membrane distillation [11], multiple-effect distillation [12], multistage flash [13], reverse osmosis [14], forward osmosis (FO) [15], multistage evacuated solar still [16], and salinity gradient power by reverse electrodialysis (SGP-RE) [17]. However, to date there are very few reports about CFD modeling of spray evaporation.

In this paper, a spraying evaporation system applied to brine disposal is reported, which is mainly used for brine disposal with concentration more than 100,000 mg/L brine. A CFD investigation has been carried out to model the brine droplet evaporation and diffusion process in hot air flow. A discrete phase model in spraying evaporation system was developed and a simulation experiment based on the gas–liquid phrase and hydromechanics theory was conducted. Furthermore, this model was verified by comparing simulation results with experimental results under different feed flow. A thorough analysis of the heat- and mass-transfer controlling steps was conducted based on this model to determine the impacts of key parameters. The system will provide a better approach to achieve the brine desalination process.

2. Experimental

2.1. Operating process

The schematic diagram of the brine spray evaporation is shown in Fig. 1. It consists five components, including heat supply system, evaporation system, feed supply system, gas system, and recovery system. Brine from feed supply system and air from gas system combined in atomizer and was mixed thoroughly. They were sprayed into droplets with large specific surface area and small diameter within 100 μm from the top of the tower. Meanwhile, hot air from heat supply system was released into the tower from the bottom and mixed with the spray droplet. During the process, water in the spray droplet absorbed thermal energy from the hot air evaporating into vapor, and the brine was concentrated into high concentration solution flowing into recycle system. After the evaporation process, the vapor was transferred by air flow out of the tower and was condensed into freshwater flowing into a tank. According to the colligative property, physical properties of solution are only related to the number of particles in solution. Therefore, brine can be substituted by sodium chloride solution in the experiment with no impact on experiment results.

2.2. Spray evaporation tower

The tower designed with the height of 2.9 m and diameter of 1 m is displayed in Fig. 2. Due to the high

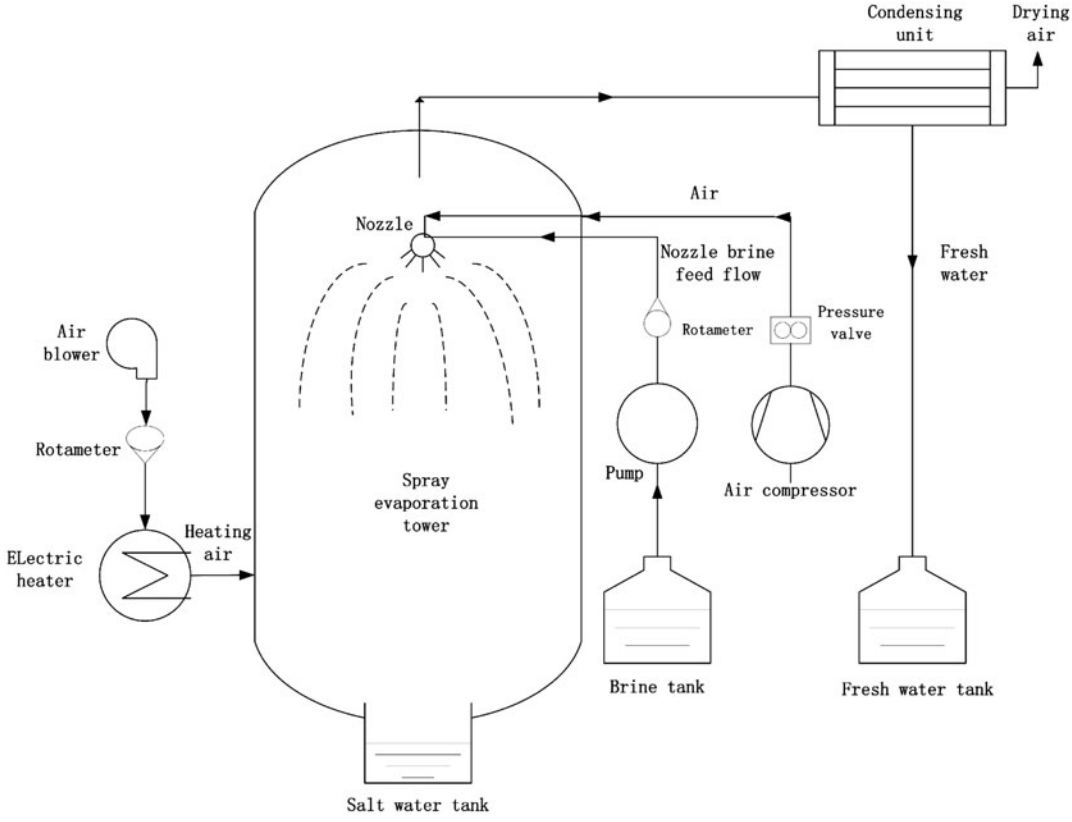

Fig. 1. Schematic diagram of the experimental set-up.

temperature and humid working conditions, the tower is made of stainless steel and is covered by 3 cm thick glass fiber insulation material to prevent the heat loss.

3. Dynamic model of the spray evaporation system

In order to visualize the temperature field distribution inside the tower, a hybrid grid method is adopted to solve the momentum, energy, and turbulence equations. The mathematical models involved in the simulation process are as follows.

3.1. Computational domain

In view of the complicated computational domain and numerous junction surfaces, the spray tower is divided into several parts, which are segmented by the grid, and a fluent procedure is used to connect the grids between each part. To obtain more accurate simulation results, the sudden change parts in shape of the tower are meshed into minimal grids. Structured grids developed by Fluent are selected to mesh the geometry in order to avoid the false diffusion problem encountered in solving the equations and reduce calculation error. To ease the effect of pressure field on velocity field, non-staggered grid is adopted. The whole model is segmented into 5.5 million grid cells. The whole tower from top to bottom is divided into five parts, and the number of grids of each part is 0.55, 1, 0.95, 2, and 1 million, respectively. Grids in the first, third, and fifth parts are structured grid and the rest parts are unstructured grid. The tower meshing and the boundary conditions as well as the dimension of the tower are clearly shown in Fig. 3(a) and cross-section meshing (z = 1.0 m from the bottom) is shown in Fig. 3(b).

3.2. Continuity equations

Fluid in any condition must be satisfied with law of conservation of mass, which can be described as continuity equation [18] as follows:

$$\frac{\partial \rho}{\partial t} + \frac{\partial \rho u}{\partial x} + \frac{\partial \rho v}{\partial y} + \frac{\partial \rho w}{\partial z} = S_m \quad (1)$$

Fig. 2. Appearance of the brine spray tower.

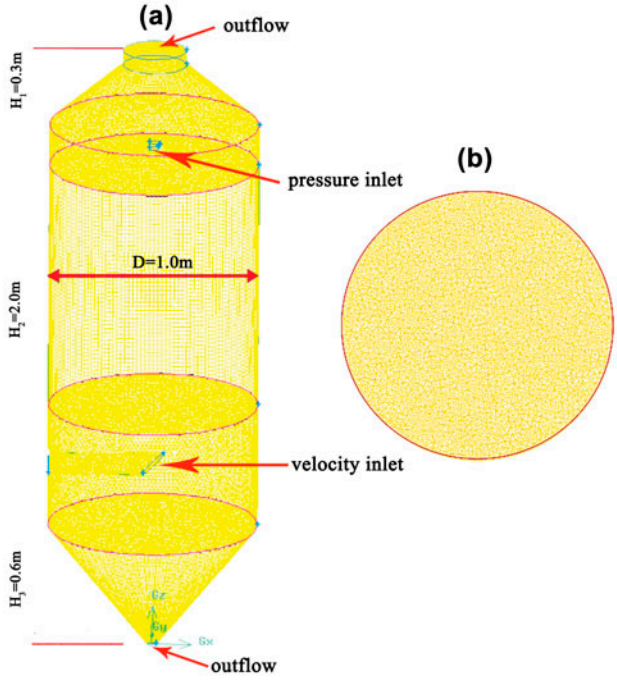

Fig. 3. Spray evaporation tower layout and schematic diagram of grid model.

Since fluid in this work is uncompressible, Eq. (1) can be substituted by:

$$div(\rho U) = 0 \tag{2}$$

3.3. Momentum equations

Law of conservation of momentum, which is Newton's second law, is the fundamental principle in governing equations. So momentum conservation equations [18] in x, y, and z-axes can be derived as the following:

$$\frac{\partial(\rho u)}{\partial t} + div(\rho u U) = -\frac{\partial p}{\partial x} + \frac{\partial \tau_{xx}}{\partial x} + \frac{\partial \tau_{yx}}{\partial y} + \frac{\partial \tau_{zx}}{\partial z} + F_x \tag{3}$$

$$\frac{\partial(\rho v)}{\partial t} + div(\rho v U) = -\frac{\partial p}{\partial y} + \frac{\partial \tau_{xy}}{\partial x} + \frac{\partial \tau_{yy}}{\partial y} + \frac{\partial \tau_{zy}}{\partial z} + F_y \tag{4}$$

$$\frac{\partial(\rho w)}{\partial t} + div(\rho w U) = -\frac{\partial p}{\partial z} + \frac{\partial \tau_{xz}}{\partial x} + \frac{\partial \tau_{yz}}{\partial y} + \frac{\partial \tau_{zz}}{\partial z} + F_z \tag{5}$$

As to uncompressible fluid with constant viscosity, Eqs. (3)–(5) can be written as:

$$\frac{\partial(\rho u)}{\partial t} + div(\rho u U) = div(\mu\ gradu) - \frac{\partial p}{\partial x} + S_u \tag{6}$$

$$\frac{\partial(\rho v)}{\partial t} + div(\rho v U) = div(\mu\ gradv) - \frac{\partial p}{\partial y} + S_v \tag{7}$$

$$\frac{\partial(\rho w)}{\partial t} + div(\rho w U) = div(\mu\ gradw) - \frac{\partial p}{\partial z} + S_w \tag{8}$$

3.4. Energy equations

Conservation of energy principle, namely the first law of thermodynamics, exists in all heat-exchange flow systems. So energy conservation equation [18] vs. temperature (T) can be obtained:

$$\frac{\partial(\rho T)}{\partial t} + div(\rho U T) = div\left(\frac{k}{c_p} grad\, T\right) + S_T \tag{9}$$

3.5. Turbulence equations

Turbulent kinetic energy equation and turbulent diffusion equation in RNGk-ε model, which is developed by Yakhot and Orszag [19], are obtained by revising large-scale movement and viscosity terms to describe the small-scale movement.

Turbulent kinetic energy equation of RNGk-ε model:

$$\frac{\partial(\rho k)}{\partial t}+\frac{\partial(\rho k u_i)}{\partial x_i}=\frac{\partial k}{\partial x_j}\left(\alpha_k \mu_{eff}\frac{\partial k}{\partial x_j}\right)+G_k-\rho\varepsilon \tag{10}$$

Turbulent diffusion equation:

$$\frac{(\rho\varepsilon)}{\partial t}+\frac{\partial(\rho\varepsilon u_i)}{\partial x_i}=\frac{\partial}{\partial x_j}\left(\alpha_\varepsilon \mu_{eff}\frac{\partial \varepsilon}{\partial x_j}\right)+C_{1\varepsilon}\cdot\frac{\varepsilon}{k}G_k-C^*_{2\varepsilon}\rho\frac{\varepsilon^2}{k} \tag{11}$$

In Eqs. (10) and (11): $\mu_{eff}=\mu+\mu_t$, $C_{2\varepsilon}=C^*_{2\varepsilon}-\frac{\eta\cdot(1-\eta/\eta_0)}{1+\beta\cdot\eta^3}$, $\eta=(2E_{ij}\cdot E_{ij})^{1/2}\cdot\frac{k}{\varepsilon}$, $E_{ij}=\frac{1}{2}\left(\frac{\partial u_i}{\partial x_j}+\frac{\partial u_j}{\partial x_i}\right)$.

The constants in Eqs. (10) and (11) are shown in Table 1.

3.6. Single-drop kinematic equations

Single-drop kinematic equations are derived from famous Basset–Boussinesq–Oseen equation [20]. Due to the high ratio of drop density to air ($\rho_p/\rho_g\approx 1{,}000$), Basset force, virtual mass force, and other unsteady state resistance can be ignored. Only taking Stokes drag into consideration, the single-drop governing equation [21] is:

$$\frac{\mathrm{d}u_{p,i}}{\mathrm{d}t}=u_{p,i} \tag{12}$$

$$\frac{\mathrm{d}u_{p,i}}{\mathrm{d}t}=\frac{f_1}{\tau_p}(u_i-u_{p,i}) \tag{13}$$

3.7. Droplet evaporation model

In view of the complication and accuracy of the model, the model based on infinite heat conduction hypothesis is adopted. Mass-transfer equation [22] can be used to describe the droplet evaporation process:

$$B_M=\frac{Y_F^{surf}-Y_F}{1-Y_F^{surf}} \tag{14}$$

Table 1
The turbulence model constants

C_u	$C_{1\varepsilon}$	$C_{2\varepsilon}$	α_k	α_ε	η_0	β
0.0845	1.42	1.68	1.39	1.39	4.377	0.012

The drop mass and temperature governing equations are:

$$\frac{\mathrm{d}m_p}{\mathrm{d}t}=-\frac{Sh}{3Sc}\frac{m_p}{\tau_p}\ln(1+B_M) \tag{15}$$

$$\frac{\mathrm{d}T_p}{\mathrm{d}t}=\frac{Nu}{3\,\mathrm{Pr}}\frac{c_{p,m}}{c_L}\frac{f_2}{\tau_p}(T_g-T_p)+\frac{\mathrm{d}m_p}{\mathrm{d}t}\frac{L_v}{m_d c_L} \tag{16}$$

$$f_2=\frac{\beta}{e^\beta-1} \tag{17}$$

$$\beta=-\frac{3Pr\tau_p}{2m_p}\frac{\mathrm{d}m_p}{\mathrm{d}t} \tag{18}$$

In consideration of the effect of convection on evaporation, Nusselt number and Sherwood number need to be revised [23] as the following:

$$Nu=2+0.552\ \mathrm{Re}_{\mathrm{slip}}^{\frac{1}{2}}Pr^{\frac{1}{3}} \tag{19}$$

$$Sh=2+0.552\ \mathrm{Re}_{\mathrm{slip}}^{\frac{1}{2}}Sc^{\frac{1}{3}} \tag{20}$$

3.8. Gas–liquid coupling model

It is known that strong mass, momentum, and energy coupling exist in the drop movement and evaporation process. Based on the droplet hypothesis, mass, momentum, and energy terms [24] in above governing equations can be substituted by:

$$S_m=-\frac{1}{V}\sum_n\frac{\mathrm{d}}{\mathrm{d}t}(m_p^n) \tag{21}$$

$$S_i=-\frac{1}{V}\sum_n\frac{d}{dt}(m_p^n u_{p,i}^n) \tag{22}$$

$$S_T=-\frac{1}{V}\sum_n\left[\frac{\mathrm{d}}{\mathrm{d}t}(m_p^n\ c_L^n\ T_d^n)-h_F^0\frac{\mathrm{d}}{\mathrm{d}t}(m_p^n)\right] \tag{23}$$

4. Simulation results and discussion

4.1. Model validation

Numerical simulations are implemented in the tower, and the boundary conditions are brine feed rate at 11, 13, and 15 L/h, respectively, feed air flux at 78 m^3/h, temperature at 260°C, air pressure given by compressor at 0.2 MPa, and the range of spray droplet

diameter within 50–100 μm calculated through the Rosin–Rammler distribution. A Fluent procedure is used to obtain the distribution of temperature field of the whole tower under different feed rate. Fig. 4 shows temperature distribution in whole spray evaporating tower under the feed rate of 11 L/h. Fig. 5 shows temperature distribution of horizontal cross section at z = 1.0 m from the bottom.

In order to verify the model, under the same boundary conditions with above simulations, temperature at five random points in the tower is measured by electric resistance thermometer when the temperature field begins to stabilize and is subsequently compared with the simulation results at the same points. The comparison is shown in Fig. 6. It can be seen that the CFD modeling data are in reasonable agreement with the experimental measured values. The relative errors are within 5%. Therefore, the model can also be used to examine the effects of air pressure given by air compressor, temperature and flux of hot air, feed rate of brine on the brine evaporation (E), and the evaporation rate (R) in the spray system. In this study, E is defined as the difference between the feed brine flux and the concentrated brine; and R is defined as the volume ratio of E to the feed brine flux.

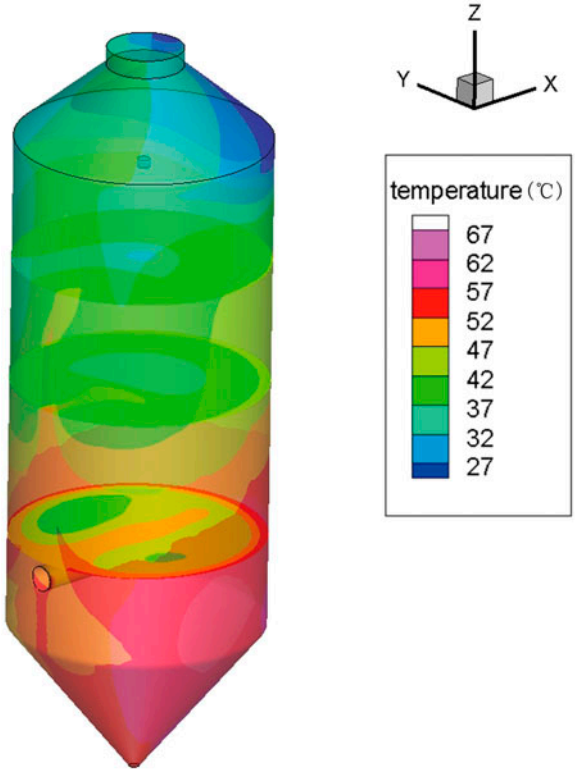

Fig. 4. Temperature distribution in spray evaporating tower under the feed rate at 11 L/h.

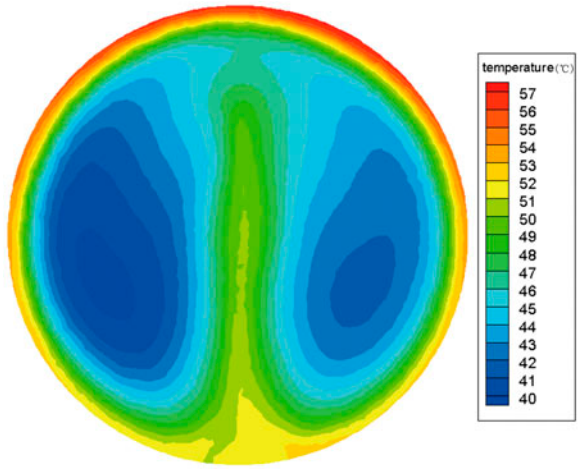

Fig. 5. Temperature distribution of cross-section at z = 1.0 m from the bottom.

4.2. Effect of compressed air pressure

The effects of air pressure on E and R are shown in Fig. 7, with the condition of hot air flux at 64 m^3/h, temperature at 200℃, and feed rate at 8 L/h. During the process P rising from 0.1 to 0.2 MPa, E and R increase rapidly and at the point of P at 0.3 MPa, E, and R have the maximum values, namely 7.23 L and 90.41%. E and R begin to fall down afterwards with continuous rising of P. The first result can be explained by the rising specific surface area of brine droplets as a result of the rising P. When the air pressure reaches 0.3 MPa, the ratio of gas to liquid in atomizing nozzle has reached equilibrium, contributing to a perfect evaporating performance. When the air pressure exceeds 0.3 MPa, the balance is broken and the droplet average diameter reached minimum size, and thus E and R begins to decrease. According to Fig. 7, it is obvious that the compressor has an appropriate operating range, namely 0.2–0.4 MPa and 0.3 MPa which are the best value for evaporating.

4.3. Effect of hot air flux

The effects of hot air flux on E and R are shown in Fig. 8 with the condition of hot air temperature at 200℃, feed rate at 8 L/h, and air pressure given by air compressor at 0.3 MPa. At first, as the air flux increases, both E and R keep rising. Nevertheless, when the air flux is between 48 and 56 m^3/h, E, and R remain steady. One reason is heat given by hot air for droplet evaporation is insufficient. The other reason is part of vapor is not blown away from spray tower by wind under the lower wind speed driven by air flux.

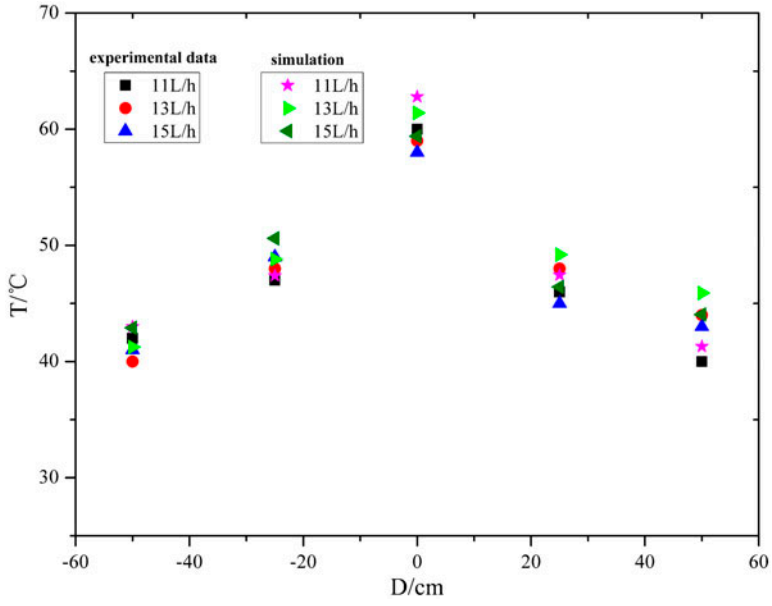

Fig. 6. Comparison of simulation temperature values with experimental ones.

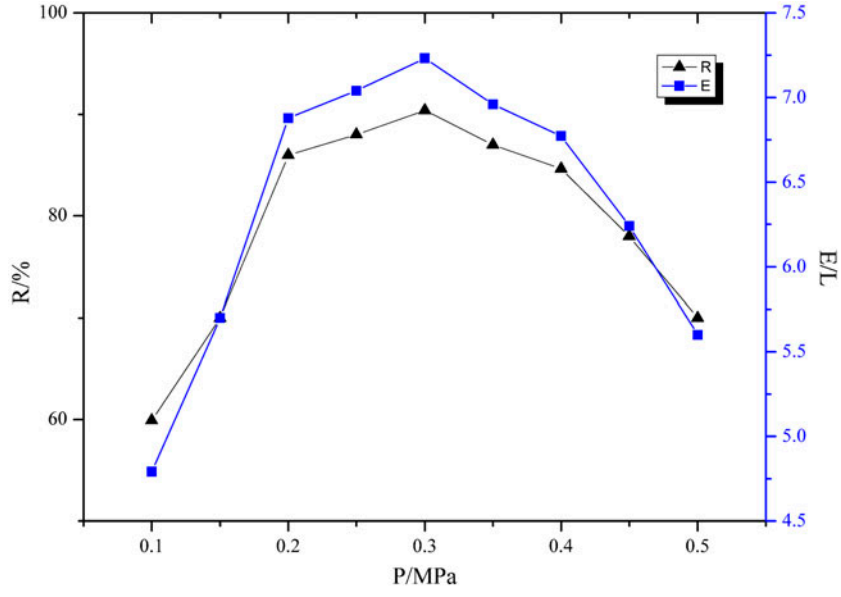

Fig. 7. Effects of air pressure given by compressor on the brine evaporation (*E*) and evaporation rate.

When the hot air flux is increased to 56 m^3/h, more heat is given to the droplet for better evaporation, which resulted in *E* and *R* rising up quickly. With the hot air flux increasing to 73 m^3/h, *R* approaches up to 90%. After that, air flux continues to increase, *E* and *R* rise slowly. Therefore, hot air flux plays an important role in the desalination efficiency of this system. The heat transferred to brine droplet as well as the vapor from brine droplet can be increased by air flux rising. But excessive air flux can result in the two following adverse effects: (1) Salt particles were blown into the condensing plant due to the high wind speed. (2) The air accounting for the mixed gas was increased, thus leading to heat-transfer residence rising and coupling with reducing the evaporation [25]. Taking into account all these factors, the best air flux is 64 m^3/h.

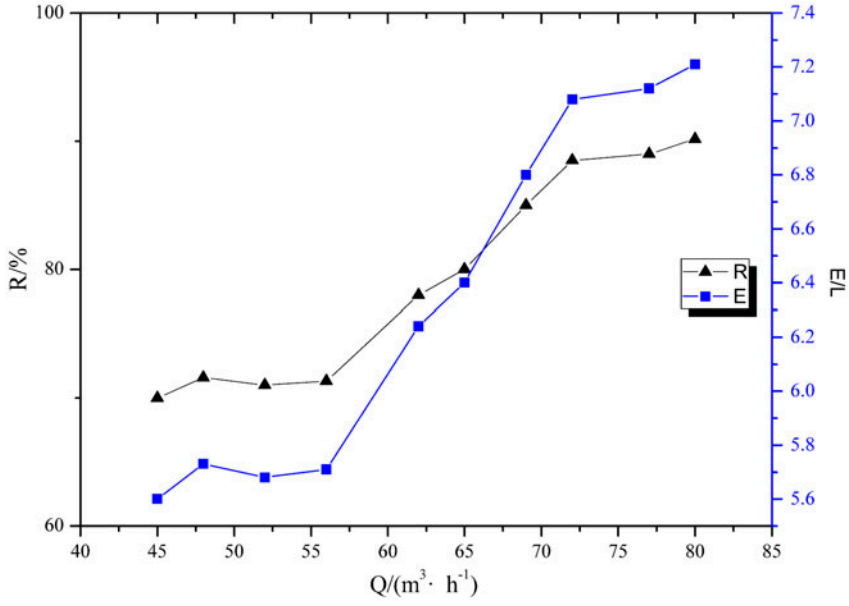

Fig. 8. Effects of heating air flux on the brine evaporation (*E*) and evaporation rate (*R*).

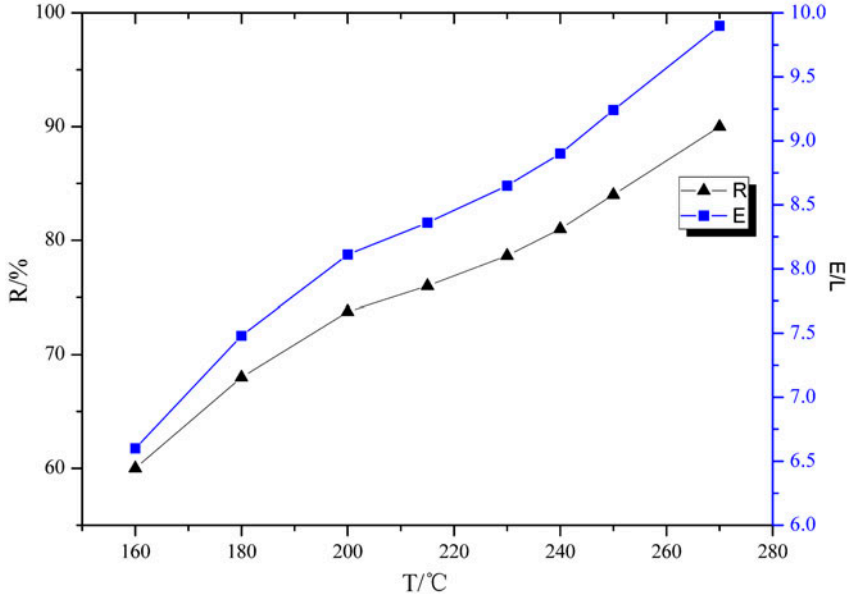

Fig. 9. Effects of temperature of heating air on the brine evaporation (*E*) and evaporation rate (*R*).

4.4. Effect of hot air temperature

Changing hot air temperature has a significant effect on evaporation under the optimized condition that hot air flux at 64 m^3/h, feed flux at 8 L/h, and compressed air pressure at 0.3 MPa, which is shown in Fig. 9. With increasing the hot air temperature, much more heat can be transferred to brine drop for evaporating, resulting in the increase in *E* and *R*. According to Fig. 9, high temperature can contribute to good evaporation results, and taking the economic factors into consideration, the perfect temperature is 270℃ in this experiment.

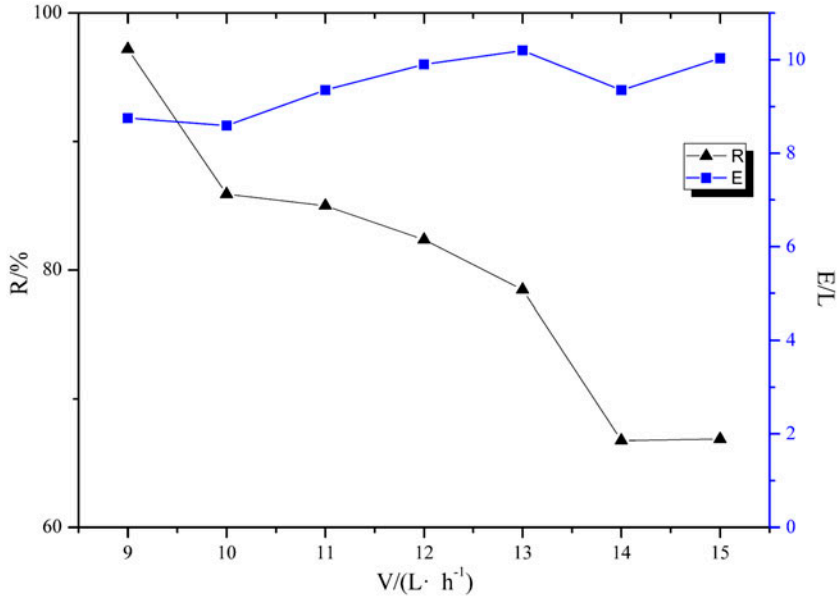

Fig. 10. Effects of feed rate on the brine evaporation (*E*) and evaporation rate (*R*).

4.5. Effect of feed rate

The effects of feed rate on *E* and *R* are shown in Fig. 10, with the condition of hot air flux at 80 m^3/h, temperature at 250℃, and compressed air pressure at 0.3 MPa. With brine feed flux increasing, *E* appears to be rising, while *R* shows a decline firstly and appears to be steady afterwards. When the feed flux is 9 L/h, *R* approaches 100%, which can be accounted for all of the spray droplets which almost evaporate due to the low feed flux. When the feed flux is within 10–12 L/h, the ratio of gas to liquid in atomizing nozzle reaches equilibrium, and a desired evaporation effect can be obtained. However, when the feed flux increases to 13 L/h, the spray droplet becomes larger because the gas–liquid equilibrium is broken. Due to its small surface area, the larger droplet cannot absorb enough heat from the hot air to evaporate and therefore fall down quickly. Besides, the feed brine droplet cannot be sprayed completely by the compressed air due to the over feed flux. The above two factors jointly cause a lower *R* 70%. The best feed flux is 11 L/h after taking both *R* and *E* into consideration.

5. Conclusions

The effects of various operating parameters on the spray evaporation system performance have been investigated. The temperature field in the spray tower is simulated. The numerical simulations have been verified by experiments with less than 5% error in predicted temperatures inside the tower. The best performance is obtained under the condition of the air pressure at 0.3 MPa, hot air temperature at 270℃, hot air flux at 64 m^3/h, and brine feed rate at 11 L/h. The CFD visualization is beneficial in the study because it can reveal the detailed temperature distribution inside the tower, which can make the experiment process understood clearly. The research showed that CFD modeling can be applied to spray evaporation process to dispose brine with high concentration and it may become a powerful tool to provide guidance for selecting the operating conditions.

Nomenclature

c_L	—	liquid heat capacity (J/(kg k))
c_p	—	specific heat capacity at constant pressure (J/(kg k))
$c_{p,m}$	—	specific heat capacity of droplets at constant pressure (J/(kg k))
f_1	—	the empirical correction of constants the Stokes resistance
f_2	—	droplet evaporation's correction factor of the droplet heating effect
G_k	—	the turbulent kinetic energy caused by buoyancy by the average velocity gradient (J)
h_F	—	gas enthalpy (J)
h_F^0	—	initial gas enthalpy (J)
k	—	thermal conductivity of air (W/(mk))
m_d	—	quality of droplets (kg)
n	—	the number of particles within the grid

Nu — Nusselt number
p — fluid pressure (Pa)
P — the pressure of the air compressor (MPa)
Pr — Prandtl number
Q — heating air volume flow (m^3/h)
R — evaporation rate (%)
S_u, S_v, S_w — source term the momentum equation is generalized (N/m^3)
S_T — source term the energy equation is generalized (W/m^3)
S_m — source term the continuity equation is generalized ($kg/(m^3\ s)$)
Sc — Schmidt number
Sh — Sherwood number
T — temperature (℃)
T_p — the temperature of liquid droplet (℃)
$\vec{U}$ — the fluid velocity vector (m/s)
u, v — fluid velocity in the x, y direction (m/s)
V — feed water flow (L/h)
w — fluid velocity in the z-direction (m/s)
Y_F — mass fraction of the fuel droplet at the position
Y_F^{surf} — droplet surface fuel mass fraction
$u_{p,j}$ — the droplet velocity (m/s)

Greek symbols

α_k — the turbulent Prandtl number in turbulent kinetic energy equation
α — the turbulent Prandtl number in dissipation rate equation
— turbulent kinetic energy dissipation rate (m^2/s^3)
μ — kinematic viscosity (kg/(ms))
μ_t — turbulent viscosity (kg/(ms))
ρ — gas density (kg/m^3)
ρ_g — droplet density (kg/m^3)
τ_p — time constant of droplets (s)

Subscripts

eff — efficient
d — droplet
p — constant pressure

Superscripts

→ — vector
* — modified value

References

[1] G.W. Lawton, C.V. Eggert, Effect of high sodium chloride concentration on trickling filter slimes, Sewage Ind. Wastes 29 (1957) 1228–1236.
[2] S. Lattemann, T. Höpner, Environmental impact and impact assessment of seawater desalination, Desalination 220 (2008) 1–15.
[3] D.H. Kim, A review of desalting process techniques and economic analysis of the recovery of salts from retentates, Desalination 270 (2011) 1–8.
[4] A. Hashim, M. Hajjaj, Impact of desalination plants fluid effluents on the integrity of seawater, with the Arabian Gulf in perspective, Desalination 182 (2005) 373–393.
[5] G.A. Tularam, M. Ilahee, Environmental concerns of desalinating seawater using reverse osmosis, J. Environ. Monit. 9 (2007) 805–813.
[6] F. Farahbod, D. Mowla, M.R. Jafari Nasr, M. Soltanieh, Experimental study of forced circulation evaporator in zero discharge desalination process, Desalination 285 (2012) 352–358.
[7] W.F. Hartman, L.J. Kepley, J. Van Fox, Apparatus and method for thermal desalination based on pressurized formation and evaporation of droplets, Google Patents 2 (2004) 12–15.
[8] M. Ben Amara, I. Houcine, A. Guizani, M. Mâalej, Experimental study of a multiple-effect humidification solar desalination technique, Desalination 170 (2004) 209–221.
[9] I. Houcine, M. Ben Amara, A. Guizani, M. Maâlej, Pilot plant testing of a new solar desalination process by a multiple-effect-humidification technique, Desalination 196 (2006) 105–124.
[10] R.D. Moita, H.A. Matos, C. Fernandes, C.P. Nunes, M.J. Pinho, Dynamic modelling and simulation of a heated brine spray system, Comput. Chem. Eng. 33 (2009) 1323–1335.
[11] H. Yu, X. Yang, R. Wang, A.G. Fane, Analysis of heat and mass transfer by CFD for performance enhancement in direct contact membrane distillation, J. Membr. Sci. 405–406 (2012) 38–47.
[12] I.S. Park, S.M. Park, J.S. Ha, Design and application of thermal vapor compressor for multi-effect desalination plant, Desalination 182 (2005) 199–208.
[13] M.K. Khamis Mansour, H.E.S. Fath, Numerical simulation of flashing process in MSF flash chamber, Desalin. Water Treat. 51 (2013) 2231–2243.
[14] S. Wardeh, H.P. Morvan, Detailed numerical simulations of flow mechanics and membrane performance in spacer-filled channels, flat and curved, Desalin. Water Treat. 1 (2009) 277–288.
[15] M.F. Gruber, C.J. Johnson, C.Y. Tang, M.H. Jensen, L. Yde, C. Hélix-Nielsen, Computational fluid dynamics simulations of flow and concentration polarization in forward osmosis membrane systems, J. Membr. Sci. 379 (2011) 488–495.
[16] Y.A. Abakr, A.F. Ismail, Theoretical and experimental investigation of a novel multistage evacuated solar still, J. Sol. Energy Eng. 127 (2005) 381–385.
[17] L. Gurreri, A. Tamburini, A. Cipollina, G. Micale, CFD analysis of the fluid flow behavior in a reverse electrodialysis stack, Desalin. Water Treat. 48 (2012) 390–403.
[18] H.K. Versteeg, W. Malalasekera, An Introduction to Computational Fluid Dynamics: The Finite Volume Method, Pearson Education, San Antonio, TX, 2007.
[19] V. Yakhot, S.A. Orszag, Renormalization group analysis of turbulence. I. Basic theory, J. Sci. Comput. 1 (1986) 3–51.

[20] T. Zhang, D. Celik, S. Van Sciver, Tracer particles for application to PIV studies of liquid helium, J. Low Temp. Phys. 134 (2004) 985–1000.
[21] C.T. Crowe, J.D. Schwarzkopf, M. Sommerfeld, Y. Tsuji, Multiphase flows with droplets and particles, second ed., CRC Press, Boca Raton, FL, 2011.
[22] M. Renksizbulut, M. Yuen, Experimental study of droplet evaporation in a high-temperature air stream, J. Heat Transfer 105 (1983) 384–388.
[23] S.S. Sazhin, Advanced models of fuel droplet heating and evaporation, Prog. Energy Combust. Sci. 32 (2006) 162–214.
[24] W.A. Sirignano, Fuel droplet vaporization and spray combustion theory, Prog. Energy Combust. Sci. 9 (1983) 291–322.
[25] R. Xiong, S. Wang, L. Xie, Z. Wang, P. Li, Experimental investigation of a baffled shell and tube desalination column using the humidification–dehumidification process, Desalination 180 (2005) 253–261.